

Systems Modeling of Ca^{2+} Homeostasis and Mobilization in Platelets Mediated by IP_3 and Store-Operated Ca^{2+} Entry

Andrew T. Dolan and Scott L. Diamond*

Institute for Medicine and Engineering, Department of Chemical and Biomolecular Engineering, University of Pennsylvania, Philadelphia, Pennsylvania

ABSTRACT Resting platelets maintain a stable level of low cytoplasmic calcium ($[\text{Ca}^{2+}]_{\text{cyt}}$) and high dense tubular system calcium ($[\text{Ca}^{2+}]_{\text{dts}}$). During thrombosis, activators cause a transient rise in inositol trisphosphate (IP_3) to trigger calcium mobilization from stores and elevation of $[\text{Ca}^{2+}]_{\text{cyt}}$. Another major source of $[\text{Ca}^{2+}]_{\text{cyt}}$ elevation is store-operated calcium entry (SOCE) through plasmalemmal calcium channels that open in response to store depletion as $[\text{Ca}^{2+}]_{\text{dts}}$ drops. A 34-species systems model employed kinetics describing IP_3 -receptor, DTS-plasmalemma puncta formation, SOCE via assembly of STIM1 and Orai1, and the plasmalemma and sarco/endoplasmic reticulum Ca^{2+} -ATPases. Four constraints were imposed: calcium homeostasis before activation; stable in zero extracellular calcium; IP_3 -activatable; and functional SOCE. Using a Monte Carlo method to sample three unknown parameters and nine initial concentrations in a 12-dimensional space near measured or expected values, we found that model configurations that were responsive to stimuli and demonstrated significant SOCE required high inner membrane electric potential (> -70 mV) and low resting IP_3 concentrations. The absence of puncta in resting cells was required to prevent spontaneous store depletion in calcium-free media. Ten-fold increases in IP_3 caused saturated calcium mobilization. This systems model represents a critical step in being able to predict platelets' phenotypes during hemostasis or thrombosis.

INTRODUCTION

The regulation of intracellular calcium is essential to numerous cellular processes. During hemostasis, platelets maintain a low resting intracellular cytoplasmic calcium ($[\text{Ca}^{2+}]_{\text{cyt}}$) as they transit through healthy vessels, yet rapidly activate and mobilize $[\text{Ca}^{2+}]_{\text{cyt}}$ to stop bleeding at injury sites. Platelet $[\text{Ca}^{2+}]_{\text{cyt}}$ mobilization is associated with integrin activation, dense (δ) and α -granule release, thromboxane A_2 synthesis, shape change, and phosphatidylserine exposure. Receptor-mediated signaling through the collagen receptor, ADP receptor (P2Y_1), thromboxane A_2 receptor, and thrombin receptors (PAR1 and PAR4 in human platelets) results in inositol [1,4,5]-trisphosphate (IP_3)-mediated Ca^{2+} release from the dense tubular system (DTS) via IP_3 -receptor (IP_3R) activation. The DTS transmembrane protein stromal interaction molecule 1 (STIM1) becomes activated as DTS calcium ($[\text{Ca}^{2+}]_{\text{dts}}$) drops, resulting in formation of clusters of STIM1-Orai1 complexes called “puncta” in regions where the DTS inner membrane is in close contact with plasmalemma membrane containing Orai1, the pore-forming unit of store-operated channels (SOCs). The STIM1-Orai1 complexes mediate store-operated Ca^{2+} entry (SOCE) to enhance the activation state of the cell (1). Platelets deficient in SOCE show reduced response to agonist-induced stimulation and impaired thrombus growth and stability under flow (2); platelets from a patient with a STIM1 mutation have shown a defect in granule secretion (3). After stimulus, $[\text{Ca}^{2+}]_{\text{cyt}}$ is then

returned to near-resting levels by the action of two ATP-dependent pumps—the plasma membrane and sarco/endoplasmic reticulum Ca^{2+} -ATPases (PMCA and SERCA). SERCA is responsible for DTS refilling.

A systems biology approach to quantify platelet homeostasis and activation must consider diverse molecular mechanisms that act in concert to regulate intracellular calcium. Platelets are an excellent tool for signal transduction studies: they are routinely available from human donors, lack a genome (obviating the need to predict gene regulation), are amenable to high throughput experiments, and present numerous druggable targets. The molecular components of Ca^{2+} regulation in the platelet include IP_3R , SERCA, calmodulin-regulated PMCA, puncta formation, and STIM1-Orai1 (Fig. 1), components that are also well represented in many other cell types. An accurate model of platelet activation may help predict hemostasis, thrombosis, or drug response.

In a prior bottom-up ordinary differential equation model (4,5), GPCR signaling through P2Y_1 activation by ADP was combined with $G\alpha_q$ activation of phospholipase C_β , phosphoinositide metabolism, PKC activation, and Ca^{2+} release by IP_3 and reuptake by the SERCA pump. With 132 fixed kinetic parameters from the literature, this model topology accurately predicted population and single cell dynamics in the absence of extracellular calcium ($[\text{Ca}^{2+}]_{\text{ex}}$) influx (as in experiments employing extracellular EDTA). Central to finding allowable initial conditions (ICs) for unknown species concentrations, the homeostasis assumption requires the IC to be a steady-state solution with low resting $[\text{Ca}^{2+}]_{\text{cyt}}$ that also allows responsiveness to elevated IP_3 .

Submitted November 4, 2013, and accepted for publication March 14, 2014.

*Correspondence: sld@seas.upenn.edu

Editor: James Sneyd.

© 2014 by the Biophysical Society
0006-3495/14/05/2049/12 \$2.00



Ca^{2+} entry from the extracellular environment is important for sustained platelet activation. This study considers the regulation of Ca^{2+} flux across the plasma membrane by SOCs, calcium channels found in many excitable and nonexcitable cell types (6). The defining characteristics of the SOCs are: low single channel conductance; high open probability; and high selectivity for Ca^{2+} (6). The known platelet copy number for many of the key constituents (7) provided a starting point for a high dimensional exploration of the model's behavior. The model accurately predicted stable resting $[\text{Ca}^{2+}]_{\text{cyt}}$ and $[\text{Ca}^{2+}]_{\text{dts}}$ as well as IP_3 -triggered Ca^{2+} mobilization in both calcium-containing and calcium-free (EDTA) extracellular buffer. Additionally, the dynamics of peripheral STIM1 and Orai1 puncta formation during activation (as a prerequisite for SOCE) was essential to predicting appropriate platelet characteristics in the presence of $[\text{Ca}^{2+}]_{\text{ex}}$.

METHODS

Model construction and simulation

The set of reactions describing the model topology (see Figs. 1 and 2 and Table 1) were modeled as a coupled set of ordinary differential equations:

$$\frac{dc}{dt} = \mathbf{f}(t); \quad (1)$$

$$\mathbf{c}(t_0 = 0) = \mathbf{c}_0.$$

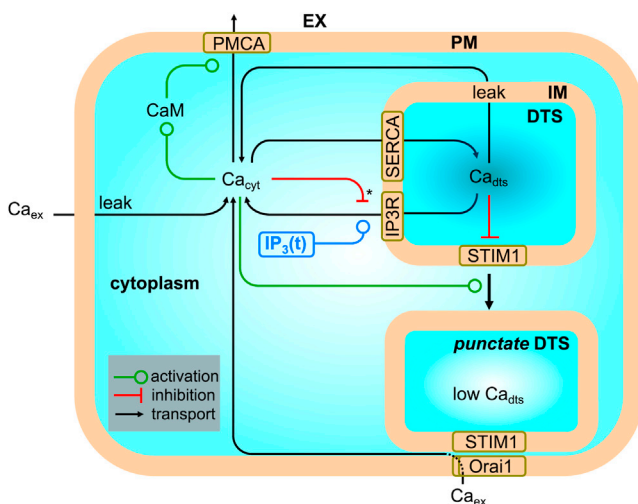


FIGURE 1 Overall model topology. The full model is comprised of 34 species, 35 reactions, 86 parameters, and five compartments. Three-dimensional compartments are the extracellular (EX), the dense-tubular system (DTS), and the cytoplasm. Two-dimensional compartments are the DTS inner membrane (IM) and the plasma membrane (PM). $[\text{Ca}^{2+}]_{\text{cyt}}$ has a biphasic influence on IP_3R activity; it stimulates IP_3R at lower concentrations and becomes inhibitory at high concentrations. $[\text{Ca}^{2+}]_{\text{cyt}}$ is also defined as a regulator of puncta formation. Puncta formation does not affect IP_3R or SERCA activity or the sizes of the DTS or IM compartments; the proteins are omitted from the punctate DTS for clarity. The system is activated by IP_3 (blue).

For reactions occurring at compartmental interfaces, concentrations of species in a two-dimensional compartment were scaled to the bulk (three-dimensional) compartment using the procedure described by Kholodenko et al. (8). Each compartment was assumed to be well mixed based on the platelet's small volume (<10 fL) (9). Except for specific cases discussed in sections to follow, reactions were modeled with either mass action kinetics or kinetics similar to Michaelis-Menten. Model simulations were performed using the SBTOOLBOX2 software package add-on for MATLAB (The MathWorks, Natick, MA) (10). All rate laws, algebraic equations, and fixed parameters listed in Table 1 were taken directly from the corresponding references.

Model overview

The calcium model (Fig. 1) comprises five compartments: the extracellular space (EX), cytosol (CYT) and dense tubular system (DTS) which are separated by the plasma membrane (PM) and DTS inner membrane (IM). Calcium is kept in balance by four major processes, which can be separated into kinetically distinct submodules, as shown in Fig. 2, A–D. In the resting platelet, a low $[\text{Ca}^{2+}]_{\text{cyt}}$ is maintained by the action of Ca^{2+} ATPases in the PM and IM. The calmodulin (CaM)-dependent Ca^{2+} transporter PMCA (Fig. 2 C) pumps Ca^{2+} into the EX, and SERCA (Fig. 2 A) pumps Ca^{2+} across the IM into the DTS. IP_3R channels (Fig. 2 B) release Ca^{2+} from the DTS into the CYT in response to a rise in $[\text{IP}_3]$. SOCs (Fig. 2 D) allow Ca^{2+} entry into the CYT across the PM in response to store depletion. Calcium pumping via SERCA was modeled using a kinetic study and model of the SERCA3b isoform (11), which is the most abundant isoform in platelets (7).

IP_3R kinetics are described with a six-state model (12) with two active conformations that are positively regulated by $[\text{IP}_3]$ and biphasically regulated by $[\text{Ca}^{2+}]_{\text{cyt}}$. Channel open probability (P_o) is based on the total number of tetrameric channels in either of the two active conformations (Table 1). For PMCA transport, we use a kinetic model of PMCA 4b, an isoform abundant in platelets and erythrocytes (7,13). PMCA independently and irreversibly transports Ca^{2+} and if bound to CaM, transports Ca^{2+} with much higher affinity and turnover rate (14,15). The volume of the platelet CYT is ~ 6 fL (16) and the volume of the DTS has been estimated to range from 1 to 10% of the CYT volume (4,17,18).

SOCE modeling

Several important features of SOCE have only recently been elucidated. SOCE activation consists of the Ca^{2+} sensor STIM1 (19,20) unbinding Ca^{2+} from its DTS-facing EF-hand domain when $[\text{Ca}^{2+}]_{\text{dts}}$ drops relative to its K_d . Calcium unbinding allows first for STIM1 oligomerization, then translocation to regions where the DTS membrane is in close apposition to the plasma membrane, and finally association with tetrameric Orai1 protein channels in the PM. Orai1 passes current when at least one dimer is bound. We model the active form of STIM1 as a STIM1 dimer (STIM_2) and model the first two steps using mass action kinetics. STIM1 dimerization is assumed to be diffusion-limited. Patch-clamp studies on larger mammalian cells indicate that store-operated current is inwardly rectifying, i.e., that the channels only allow current into the cell and do not operate in reverse under physiological conditions (21).

Platelets possess several other isoforms of STIM and Orai (7,22). Of these, STIM1 and Orai1 are the best studied, and they are the most likely candidates for the components of functional SOC channels. For the purpose of this study, thenceforth, we will refer to STIM1 and Orai1 as simply “STIM” and “Orai”.

Puncta formation

STIM and Orai are localized in separate membranes that require close contact for SOC activation (23,24). Store depletion causes STIM and Orai to undergo a rearrangement from being diffusely distributed in their

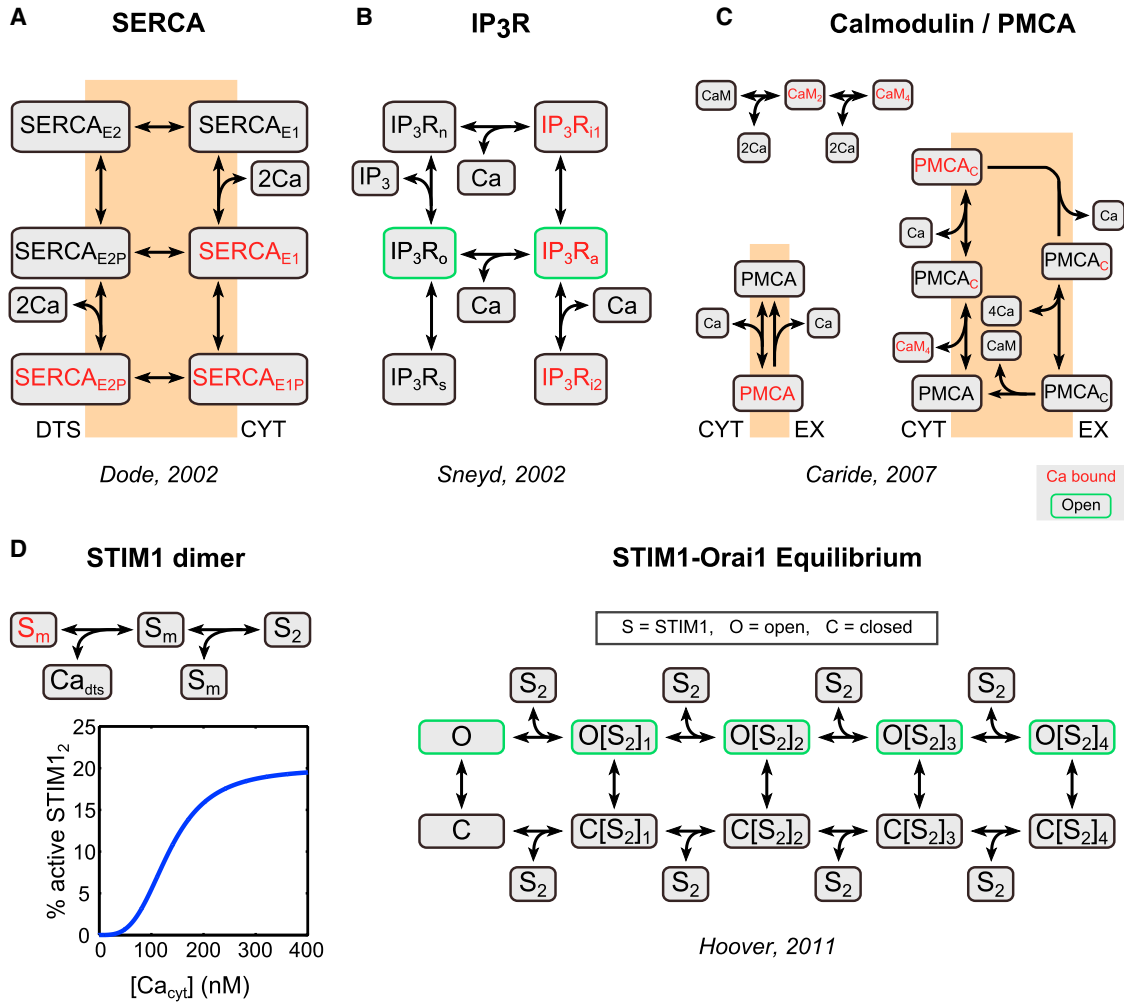


FIGURE 2 Submodule schematics and calcium current equation. (A) SERCA transport. Subscripts: *E1*, facing cytosol; *E2*, facing DTS; and *P*, phosphorylated. (B) IP₃R dynamics. Subscripts: *n*, native; *il*, inhibited; *o*, open; *a*, active; *s*, shut; and *i2*, inhibited. (C) PMCA transport. PMCA can irreversibly transport Ca²⁺ independently (slow) or with CaM as a cofactor (fast). Subscripts: *C*, calmodulin bound; *2*, two Ca²⁺ ions bound; and *4*, four Ca²⁺ ions bound. (D) SOC assembly and dynamics. Calcium dissociation results in Ca²⁺_{cyt}-dependent translocation of dimerized STIM to form puncta. STIM in the puncta instantaneously equilibrates with Orai according to a set of Monod-Wyman-Changeux equilibrium relationships determined by Hoover et al. (18). Subscripts: *m*, monomeric STIM; and *2*, dimeric STIM. (Arrow with two arrowheads) Reversible reaction; (single arrowhead) irreversible reaction. (Red text) Ca²⁺ is bound. (Green outline) Channel is open.

respective membranes to a colocalized state at junctions between the IM and PM called puncta (19). STIM can form puncta by two mechanisms. One is passive diffusion ($D \sim 0.1\text{--}0.15 \mu\text{m}^2/\text{s}$) (25). This mechanism accounts well for the time lag between STIM oligomerization and puncta formation in larger mammalian cells (26); however, platelets are small enough that timescales for diffusion-limited translocation would be <1 s. When STIM puncta entry was modeled in this fashion (i.e., STIM in the puncta is essentially equal to total bulk STIM due to fast diffusion), we observed that the simulation could not satisfy homeostatic constraints on Ca²⁺ while also simultaneously observing significant contribution of SOCE to [Ca²⁺]_{cyt} after IP₃ stimulus. Thus, we modeled STIM₂ entry into puncta with a [Ca²⁺]_{cyt}-dependent Hill function applied to bulk IM STIM₂:

$$(STIM_2)_p = \theta_p \times STIM_2,$$

$$\theta_p = \alpha \left(\frac{[Ca^{2+}]_{cyt}^n}{K_M^n + [Ca^{2+}]_{cyt}^n} \right) + 0.01. \quad (2)$$

Only STIM dimers (STIM₂) are allowed to enter the puncta based on evidence that STIM oligomerization precedes puncta formation (26). Equation 2 effectively reduces the amount of STIM₂ available for binding to Orai because only STIM in the puncta ((STIM₂)_p) is able to interact with Orai. The parameter α represents the maximum fraction of STIM₂ that can enter the puncta and was set to 0.2. K_M is the value of [Ca²⁺]_{cyt} at which θ_p is 50% of the maximum and n is the Hill coefficient. The offset of 0.01 is needed to prevent $\theta_p \ll 1$ at rest, leading to scenarios where [Ca²⁺]_{cyt} is the more dominant regulator of SOCE activity than [Ca²⁺]_{dts}. This regulation could represent an unidentified scaffold or helper protein that is regulated by [Ca²⁺]_{cyt} and necessary for STIM₂ puncta entry. Alternatively, it also could represent an increase in the amount of surface contact between the IM and PM as a result of actin-dependent cytoskeletal reorganization (27).

Channel assembly

A recent study employing Orai tetramers fused with variable numbers of STIM dual C-terminal domains has shown a graded relationship between

TABLE 1 Reaction equations, rate laws, and kinetic constants

Reaction / Quantity	Mechanism	Rate Law / Rule	Parameter Values	Ref.
SERCA shuttling	$SERCA_{E2} \leftrightarrow SERCA_{E1}$	$k_1 \cdot [SERCA_{E2}] - k_{-1} \cdot [SERCA_{E1}]$	$k_1 = 600 \text{ s}^{-1}, k_{-1} = 600 \text{ s}^{-1}$	(11)
Ca^{2+} binding SERCA	$SERCA_{E1} + 2 Ca^{2+}_{cyt} \leftrightarrow SERCA_{E1} \cdot Ca^{2+}$	$k_1 \cdot [SERCA_{E1}] \cdot [Ca^{2+}_{cyt}]^2 - [Ca^{2+}_{cyt}]^2 \cdot [SERCA_{E1} \cdot Ca^{2+}]$	$k_1 = 1 \times 10^{15} \text{ M}^{-2} \text{ s}^{-1}, k_{-1} = 10 \text{ s}^{-1}$	(11)
Phosphorylation of SERCA	$SERCA_{E1} \cdot Ca^{2+} \leftrightarrow SERCA_{E1} \cdot P \cdot Ca^{2+}$	$k_1 \cdot [SERCA_{E1} \cdot Ca^{2+}] - k_{-1} \cdot [SERCA_{E1} \cdot P \cdot Ca^{2+}]$	$k_1 = 700 \text{ s}^{-1}, k_{-1} = 5 \text{ s}^{-1}$	(11)
Ca^{2+} transport across IM	$SERCA_{E1} \cdot P \cdot Ca^{2+} \leftrightarrow SERCA_{E1} \cdot P \cdot Ca^{2+}$	$k_1 \cdot [SERCA_{E1} \cdot P \cdot Ca^{2+}] - k_{-1} \cdot [SERCA_{E1} \cdot P \cdot Ca^{2+}]$	$k_1 = 600 \text{ s}^{-1}, k_{-1} = 50 \text{ s}^{-1}$	(11)
Ca^{2+} release into DTS	$SERCA_{E2} \cdot P \cdot Ca^{2+} \leftrightarrow SERCA_{E2} \cdot P + 2 Ca^{2+}_{dts}$	$k_1 \cdot [SERCA_{E2} \cdot P \cdot Ca^{2+}] - k_{-1} \cdot [SERCA_{E2} \cdot P] \cdot [Ca^{2+}_{dts}]^2$	$k_1 = 1000 \text{ s}^{-1}, k_{-1} = 4 \times 10^9 \text{ M}^{-2} \text{ s}^{-1}$	(11)
SERCA dephosphorylation	$SERCA_{E2} \cdot P \leftrightarrow SERCA_{E2}$	$k_1 \cdot [SERCA_{E2} \cdot P] - k_{-1} \cdot [SERCA_{E2}]$	$k_1 = 500 \text{ s}^{-1}, k_{-1} = 1 \text{ s}^{-1}$	(11)
IP ₃ R inhibition	$IP_3R_n + Ca^{2+}_{cyt} \leftrightarrow IP_3R_n$	$[IP_3R_n] \cdot ((k_1 \cdot L_1 + I_2) \cdot [Ca^{2+}_{cyt}] / (L_1 + [Ca^{2+}_{cyt}]) - (1 + L_1 / L_3)) - [IP_3R_n] \cdot (k_{-1} + I_2)$	$k_1 = 0.64 \text{ s}^{-1} \mu\text{M}^{-1}, L_1 = 0.12 \mu\text{M}, I_2 = 1.7 \text{ s}^{-1}$ $L_3 = 0.025 \mu\text{M}, k_{-1} = 0.04 \text{ s}^{-1}, I_2 = 0.8 \text{ s}^{-1}$	(12)
IP ₃ R binding IP ₃	$IP_3R_n + IP_3 \leftrightarrow IP_3R_n$	$[IP_3R_n] \cdot ([IP_3] \cdot ((k_2 \cdot L_3 + I_4 \cdot [Ca^{2+}_{cyt}]) / (L_3 + [Ca^{2+}_{cyt}]) - (1 + L_3 / L_1))) - [IP_3R_n] \cdot ((k_2 + I_4) \cdot [Ca^{2+}_{cyt}] / (1 + [Ca^{2+}_{cyt}] / L_5))$	$k_2 = 37.4 \text{ s}^{-1} \mu\text{M}^{-1}, I_4 = 1.7 \text{ s}^{-1} \mu\text{M}^{-1}$ $k_2 = 1.4 \text{ s}^{-1}, I_4 = 2.5 \mu\text{M}^{-1} \text{ s}^{-1}, L_5 = 54.7 \mu\text{M}$	(12)
IP ₃ R activation	$IP_3R_n + Ca^{2+}_{cyt} \leftrightarrow IP_3R_n$	$[IP_3R_n] \cdot ((k_4 \cdot L_5 + I_6) \cdot [Ca^{2+}_{cyt}] / (L_5 + [Ca^{2+}_{cyt}])) - [IP_3R_n] \cdot (k_4 + I_6)$	$k_4 = 4 \text{ s}^{-1} \mu\text{M}^{-1}, I_6 = 4707 \text{ s}^{-1}$	(12)
IP ₃ R inhibition	$IP_3R_n \cdot (k_1 \cdot L_1 + I_2) \cdot [Ca^{2+}_{cyt}] / (L_1 + [Ca^{2+}_{cyt}]) - [IP_3R_n] \cdot (k_{-1} + I_2)$	$[IP_3R_n] \cdot ((k_1 \cdot L_1 + I_2) \cdot [Ca^{2+}_{cyt}] / (L_1 + [Ca^{2+}_{cyt}]) - [IP_3R_n] \cdot (k_{-1} + I_2))$	$k_1 = 0.54 \text{ s}^{-1} \mu\text{M}^{-1}, I_2 = 11.4 \text{ s}^{-1}$	(12)
IP ₃ R closing	$IP_3R_n \cdot (k_3 \cdot L_5 / (L_5 + [Ca^{2+}_{cyt}])) - [IP_3R_n] \cdot k_{-3}$	$[IP_3R_n] \cdot (k_3 \cdot L_5 / (L_5 + [Ca^{2+}_{cyt}])) - [IP_3R_n] \cdot k_{-3}$	$k_3 = 11 \text{ s}^{-1} \mu\text{M}^{-1}, k_{-3} = 29.8 \text{ s}^{-1}$	(12)
Channel open probability (P_{open})	$(0.9 \cdot IP_3R_n / IP_3R_{\text{total}} + 0.1 \cdot pIP_3R_n / IP_3R_{\text{total}}) \cdot RT / zF \cdot \ln([Ca^{2+}_{cyt}] / [Ca^{2+}_{dts}])$	$(0.9 \cdot IP_3R_n / IP_3R_{\text{total}} + 0.1 \cdot pIP_3R_n / IP_3R_{\text{total}}) \cdot RT / zF \cdot \ln([Ca^{2+}_{cyt}] / [Ca^{2+}_{dts}])$	$k_3 = 11 \text{ s}^{-1} \mu\text{M}^{-1}, k_{-3} = 29.8 \text{ s}^{-1}$	(12)
IM potential (ψ_{IM})	$N_{\text{IP3R}} \cdot P_{\text{open}} \cdot Y_{\text{IP3R}} \cdot e^{-\psi_{\text{IM}}} - \psi_{\text{IM}}$	$N_{\text{IP3R}} \cdot P_{\text{open}} \cdot Y_{\text{IP3R}} \cdot e^{-\psi_{\text{IM}}} - \psi_{\text{IM}}$	$Y_{\text{IP3R}} = 10 \text{ pS}$	(30)
Ca^{2+} release from DTS via IP ₃ R	$Ca^{2+}_{dts} \leftrightarrow Ca^{2+}_{cyt}$	$k_1 \cdot [STIM1] \cdot [Ca^{2+}_{dts}] - k_{-1} \cdot [STIM1 \cdot Ca^{2+}]$	$k_{-1} / k_1 = 200 \mu\text{M}$	(1)
Ca^{2+} dis binding STIM1	$STIM1 + Ca^{2+}_{dts} \leftrightarrow STIM1 \cdot Ca^{2+}_{dts}$	$k_1 \cdot [STIM1] \cdot [Ca^{2+}_{dts}] - k_{-1} \cdot [STIM1 \cdot Ca^{2+}]$	$k_1 = 9 \times 10^8 \text{ s}^{-1} \text{M}^{-1}, k_{-1} = 3.5 \text{ s}^{-1}$	This study
STIM1 dimerization	$2 STIM1 \leftrightarrow STIM1_2$	$\alpha \cdot [Ca^{2+}_{cyt}]^2 / ([Ca^{2+}_{cyt}] + K_{\text{dimer}}) + 0.01$	$K_{\text{dimer}} = 100 - 300 \text{ nM}, n = 0.5 - 3, \alpha = 0.2$	This study
Puncta formation factor (θ_p)	$STIM1_2 \leftrightarrow (STIM1_2)_p$	$[STIM1_2] \cdot \theta_p$		
STIM in puncta binding Ora1	$(STIM1_2)_p + Ora1 \leftrightarrow (STIM1_2)_p \cdot Ora1$	see equations below		
Orai (closed) with 1 STIM1 ₂ bound	$4 \cdot K_a \cdot [C] \cdot [S]$	$4 \cdot K_a \cdot [C] \cdot [S]$	$K_a = 100$	(18)
Orai (closed) with 2 STIM1 ₂ bound	$3/2 \cdot K_a \cdot a \cdot [OS] \cdot [S]$	$3/2 \cdot K_a \cdot a \cdot [OS] \cdot [S]$	$a = 0.5$	(18)
Orai (closed) with 3 STIM1 ₂ bound	$2/3 \cdot K_a \cdot a^2 \cdot [CS_2] \cdot [S]$	$2/3 \cdot K_a \cdot a^2 \cdot [CS_2] \cdot [S]$		(18)
Orai (closed) with 4 STIM1 ₂ bound	$1/4 \cdot K_a \cdot a^3 \cdot [CS_3] \cdot [S]$	$1/4 \cdot K_a \cdot a^3 \cdot [CS_3] \cdot [S]$		(18)
Orai (open) with 0 STIM1 ₂ bound	$L \cdot [C]$	$L \cdot [C]$	$L = 0.0001$	(18)
Orai (open) with 1 STIM1 ₂ bound	$4 \cdot K_a \cdot f \cdot [O] \cdot [S]$	$4 \cdot K_a \cdot f \cdot [O] \cdot [S]$	$f = 1420$	(18)
Orai (open) with 2 STIM1 ₂ bound	$3/2 \cdot K_a \cdot f \cdot a \cdot [OS] \cdot [S]$	$3/2 \cdot K_a \cdot f \cdot a \cdot [OS] \cdot [S]$		(18)
Orai (open) with 3 STIM1 ₂ bound	$2/3 \cdot K_a \cdot f \cdot a^2 \cdot [OS_2] \cdot [S]$	$2/3 \cdot K_a \cdot f \cdot a^2 \cdot [OS_2] \cdot [S]$		(18)
Orai (open) with 4 STIM1 ₂ bound	$1/4 \cdot K_a \cdot f \cdot a^3 \cdot [OS_3] \cdot [S]$	$1/4 \cdot K_a \cdot f \cdot a^3 \cdot [OS_3] \cdot [S]$		(18)
Orai (open) with 4 STIM1 ₂ bound (STIM1 ₂) _p mass balance	$[S] + [CS] + 2 \cdot [CS_2] + 3 \cdot [CS_3] + 4 \cdot [CS_4] + [OS] + [OS_2] + [OS_3] + 4 \cdot [OS_4]$	$[S] + [CS] + 2 \cdot [CS_2] + 3 \cdot [CS_3] + 4 \cdot [CS_4] + [OS] + [OS_2] + [OS_3] + 4 \cdot [OS_4]$		(18)
Orai1 mass balance	$[C] + [CS] + [CS_2] + [CS_3] + [CS_4] + [OS] + [OS_2] + [OS_3] + [OS_4] + [OS_4] + [OS_4]$	$[C] + [CS] + [CS_2] + [CS_3] + [CS_4] + [OS] + [OS_2] + [OS_3] + [OS_4] + [OS_4] + [OS_4]$		(18)
PM potential (ψ_{PM})	$RT / zF \cdot \ln([Ca^{2+}_{ex}] / [Ca^{2+}_{cyt}])$	$RT / zF \cdot \ln([Ca^{2+}_{ex}] / [Ca^{2+}_{cyt}])$	$Y_{\text{SOC}} = 0.02 \text{ pS}$	(18, 6)
Calcium entry via SOC channels	$Ca^{2+}_{ex} \leftrightarrow Ca^{2+}_{cyt}$	$Y_{\text{SOC}} \cdot e^{-\psi_{\text{PM}}} - \psi_{\text{PM}} \cdot \sum_i (OS_i)$	$k_1 = 1 \times 10^7 \text{ s}^{-1} \text{M}^{-1}, k_{-1} = 50 \text{ s}^{-1}$	(14)
PMCA binding cytosolic Ca	$Ca^{2+}_{cyt} + PMCA \leftrightarrow Ca^{2+} \cdot PMCA$	$k_1 \cdot [PMCA] \cdot [Ca^{2+}_{cyt}] - k_{-1} \cdot [Ca^{2+} \cdot PMCA]$	$k_1 = 5.5 \text{ s}^{-1}$	(14)
PMCA releasing Ca into EX	$Ca^{2+} \cdot PMCA \rightarrow PMCA + Ca^{2+}_{ex}$	$k_1 \cdot [Ca^{2+} \cdot PMCA]$		(14)
First two Ca^{2+} binding CaM	$CaM + 2 Ca^{2+}_{cyt} \leftrightarrow Ca^{2+}_2 \cdot CaM$	$k_1 \cdot [CaM] \cdot [Ca^{2+}_{cyt}]^2 - k_{-1} \cdot [Ca^{2+}_2 \cdot CaM]$	$k_1 = 2.669 \times 10^{12} \text{ s}^{-1} \text{M}^{-2}, k_{-1} = 2.682 \text{ s}^{-1}$	(14)
Second two Ca^{2+} binding CaM	$Ca^{2+}_2 \cdot CaM + 2 Ca^{2+}_{cyt} \leftrightarrow Ca^{2+}_4 \cdot CaM$	$k_1 \cdot [CaM \cdot Ca^{2+}_2] \cdot [Ca^{2+}_{cyt}]^2 - k_{-1} \cdot [Ca^{2+}_4 \cdot CaM]$	$k_1 = 1.704 \times 10^{14} \text{ s}^{-1} \text{M}^{-2}, k_{-1} = 1.551 \text{ s}^{-1}$	(14)
CaM binding and activating PMCA	$PMCA + Ca^{2+}_4 \cdot CaM \leftrightarrow PMCA \cdot (Ca^{2+}_4 \cdot CaM)$	$k_1 \cdot [CaM \cdot Ca^{2+}_4] \cdot [PMCA] - k_{-1} \cdot [PMCA \cdot (Ca^{2+}_4 \cdot CaM)]$	$k_1 = 2 \times 10^5 \text{ s}^{-1} \text{M}^{-1}, k_{-1} = 0.0008 \text{ s}^{-1}$	(14)
PMCA/CaM binding cytosolic Ca	$PMCA \cdot (Ca^{2+}_4 \cdot CaM) + Ca^{2+}_{cyt} \leftrightarrow PMCA \cdot (Ca^{2+}_4 \cdot CaM) \cdot Ca^{2+}_{cyt}$	$k_1 \cdot [PMCA \cdot (Ca^{2+}_4 \cdot CaM)] \cdot [Ca^{2+}_{cyt}] - k_{-1} \cdot [PMCA \cdot (Ca^{2+}_4 \cdot CaM) \cdot Ca^{2+}_{cyt}]$	$k_1 = 5 \times 10^7 \text{ s}^{-1} \text{M}^{-1}, k_{-1} = 10 \text{ s}^{-1}$	(14)
PMCA/CaM releasing Ca into EX	$PMCA \cdot (Ca^{2+}_4 \cdot CaM) \cdot Ca^{2+}_{cyt} \rightarrow PMCA \cdot (Ca^{2+}_4 \cdot CaM) + Ca^{2+}_{ex}$	$k_1 \cdot [PMCA \cdot (Ca^{2+}_4 \cdot CaM) \cdot Ca^{2+}_{cyt}]$	$k_1 = 30 \text{ s}^{-1}$	(14)
Release of Ca^{2+}_{cyt} bound to CaM	$PMCA \cdot (Ca^{2+}_4 \cdot CaM) \leftrightarrow PMCA \cdot CaM + 4 Ca^{2+}_{cyt}$	$k_1 \cdot [PMCA \cdot (Ca^{2+}_4 \cdot CaM)] - k_{-1} \cdot [PMCA \cdot CaM] \cdot [Ca^{2+}_{cyt}]^4$	$k_1 = 10 \text{ s}^{-1}, k_{-1} = 7.332 \times 10^{20} \text{ s}^{-1} \text{M}^{-4}$	(14)
Dissociation of PMCA and CaM	$PMCA \cdot CaM \rightarrow PMCA + CaM$	$k_1 \cdot [PMCA \cdot CaM]$	$k_1 = 0.033 \text{ s}^{-1}$	(14)
Calcium leak across IM	$Ca^{2+}_{dts} \leftrightarrow Ca^{2+}_{cyt}$	$k_1 \cdot ([Ca^{2+}_{dts}] - [Ca^{2+}_{cyt}])$	$k_1 = 0.003333 \text{ s}^{-1}$	(32)
Calcium leak across PM	$Ca^{2+}_{ex} \leftrightarrow Ca^{2+}_{cyt}$	$S_{\text{leak}} \cdot Y_{\text{leak}} - \psi_{\text{PM}}$	$Y_{\text{leak}} = 0.7 \text{ pS} \cdot \text{m}^{-2}$	(4)

the number of STIM₂ bound and the activation state of the SOC channel (28). To model association of (STIM₂)_p with Orai, we adopt a similar Monod-Wyman-Changaux (MWC) (18,29) equilibrium framework to model cooperative ligand binding. Channels exist in four states having 0–4 STIM₂ bound. Each channel state can either be open (O, OS, OS₂, OS₃, OS₄) or closed (C, CS, CS₂, CS₃, CS₄). (STIM₂)_p binds to Orai tetramers with negative cooperativity and channels open with positive cooperativity as a function of the number of (STIM₂)_p bound. All states have the same conductance, but only open channels can pass current. At any given instant, not all (STIM₂)_p is bound to Orai. The concentration of (STIM₂)_p accessible to (i.e., in the puncta) but not bound to Orai is called S_f and is obtained by mass balance. Fig. 2 D shows the possible transitions that can occur among these 10 states; the equations corresponding to these relationships are given in Table 1. General equations to represent the equilibrium relationships are

$$\begin{aligned} O &= L/C; \quad i = 0, \\ OS_i &= OS_{i-1} \left(\frac{4 - (i - 1)}{i} \right) f a^i K_a S_f; \quad i = 1 : 4. \end{aligned} \quad (3)$$

In these equations, L is the intrinsic opening equilibrium constant, K_a is the association constant for (STIM₂)_p binding, a is the binding cooperativity factor, and f is the opening cooperativity factor (18). Similar equations can be written for the closed states. Using a procedure similar to that of Hoover et al. (18), we generated analytic solutions to these nine nonlinear equations coupled with mass balances on total (STIM₂)_p and Orai using the MATLAB Symbolic Toolbox. These algebraic equations are in terms of Orai and S_f . We used a linear set search algorithm to search for values of S_f which give the correct solutions for sets of pairs of Orai and (STIM₂)_p. The result was a two-dimensional lookup table that returns S_f as a function of Orai and (STIM₂)_p. With S_f in hand, the channel states can be calculated from the analytic solutions to the MWC equations. Fig. S1 A in the Supporting Material illustrates the relationship between the total number of open channels, and (STIM₂)_p and Orai.

Modeling ion channel current and membrane potential

The driving force across an ion channel embedded in a biological membrane is the difference between the electrical potential across the membrane (E_m) and the reversal potential of the ion, which is given by the Nernst equation (30). Net Ca²⁺ current is therefore given by

$$I = \gamma N P_o N_A / F \left(- \frac{RT}{zF} \ln \left(\frac{[Ca^{2+}]_{out}}{[Ca^{2+}]_{in}} \right) + E_m \right). \quad (4)$$

N is the total number of channels per platelet, γ is the single channel conductance, P_o is the channel open probability, and z is the number of elementary charges per ion (two in the case of Ca²⁺). The quantity N_A/F (Avogadro's number divided by the Faraday constant) represents the number of elementary charges per second per Ampere of current and is necessary to convert from units of current to moles of Ca²⁺ per second. In this general equation, $[Ca^{2+}]_{out}$ represents the Ca²⁺ concentration in the outer compartment and $[Ca^{2+}]_{in}$ represents Ca²⁺ concentration in the inner compartment, e.g., for SOCs $[Ca^{2+}]_{out} = [Ca^{2+}]_{ex}$ and $[Ca^{2+}]_{in} = [Ca^{2+}]_{cyt}$. For purposes of determining SOC current, the product $N \times P_o$ is equal to the total number of open channels, which is obtained from the MWC equations listed in Eq. 3. This scheme for calculating SOC current is summarized in Fig. S1 B.

Using the Hodgkin and Huxley framework, the plasma membrane is modeled as an resistor-capacitor circuit where fluxes of different ions

are considered to be a set of resistors in parallel. We arrive at the following equation for modeling the change in membrane potential over time (31):

$$\frac{dE_m}{dt} = \frac{1}{C_M} \times I_{Ca}. \quad (5)$$

Calcium flow across the membrane, I_{Ca} , is the sum of all sources of current such as flow through pumps, channels, or passive leakage (32). The specific membrane capacitance, C_M , is a relatively conserved quantity across cell types (33) and for this study is estimated to be $\sim 2 \mu\text{F}/\text{cm}^2$ based on whole-cell patch-clamp measurements that suggest platelet specific capacitance is somewhat higher than the $1 \mu\text{F}/\text{cm}^2$ value typically seen in other cell types due to platelets' extensive surface invaginations (34). Resting potential across the plasma membrane is maintained by voltage-dependent K⁺ channels and has been estimated with voltage-sensitive fluorescent dyes to be between -60 and -70 mV (35–37). In practice in human platelets, plasma membrane potential (V_{PM}) is fairly constant during platelet activation by common agonists (37). The resting potential across the DTS membrane (V_{IM}) is much less certain, and remains unmeasured. The fact that slow Ca²⁺ leakage from the endoplasmic reticulum is observed in the presence of SERCA inhibitors implies resting V_{IM} is more inside-negative than the reversal potential of Ca²⁺ across the IM. Assuming a resting $[Ca^{2+}]_{dts}$ of $300 \mu\text{M}$, V_{IM} must be > -100 mV (38). For experiments in mouse pancreatic acinar cells (39) and rat sensory neurons (40) in which $[Ca^{2+}]_{cyt}$ was held constant with a BAPTA/Ca²⁺ buffer solution, Ca²⁺ stores were depleted using SERCA inhibitors and store Ca²⁺ content was measured with Mag-Fura2. It was found that stores plateau at a level greater than clamped $[Ca^{2+}]_{cyt}$. Assuming these plateaus are the result of net zero flux out of IM Ca²⁺ channels, from Eq. 4 one can calculate a V_{IM} as high as -74 mV.

IP₃ forcing function

Agonist-stimulated generation of IP₃ is well studied and has been previously modeled (4). For this study, in which we explore combined IP₃-mediated and SOCE regulation of intracellular Ca²⁺, we removed upstream pathways leading to IP₃ generation to simplify the modeling process and reduce the number of unknowns requiring estimation. We impose an explicitly defined supply of [IP₃] as a forcing function over time to simulate an activated platelet. We constructed a piecewise polynomial function to model [IP₃] in which IP₃ rises to approximately fivefold its resting value within 5 s of stimulation, and returns to a new steady level within 200 s. The level of resting [IP₃] varies with the model resting state (see Fig. 3 C). Fig. S2 illustrates these curves.

RESULTS

Platelet calcium balance

At rest, the platelet maintains stable submicromolar levels (40–100 nM) (36) of Ca²⁺_{cyt} in balance with: nanomolar levels of IP₃ (41–43); high submillimolar Ca²⁺_{dts} (100–400 μM); and millimolar Ca²⁺_{ex} (~ 2 mM). In achieving Ca²⁺ homeostasis, the cell must balance the four interacting molecular modules: IP₃R, SERCA, PMCA, and SOCE. Additionally, at the moment of GPCR activation, the dynamics of IP₃ synthesis and conversion mediate a large increase in $[Ca^{2+}]_{cyt}$ that is typically restored to resting levels while the Ca²⁺ store refills after store-operated calcium entry.

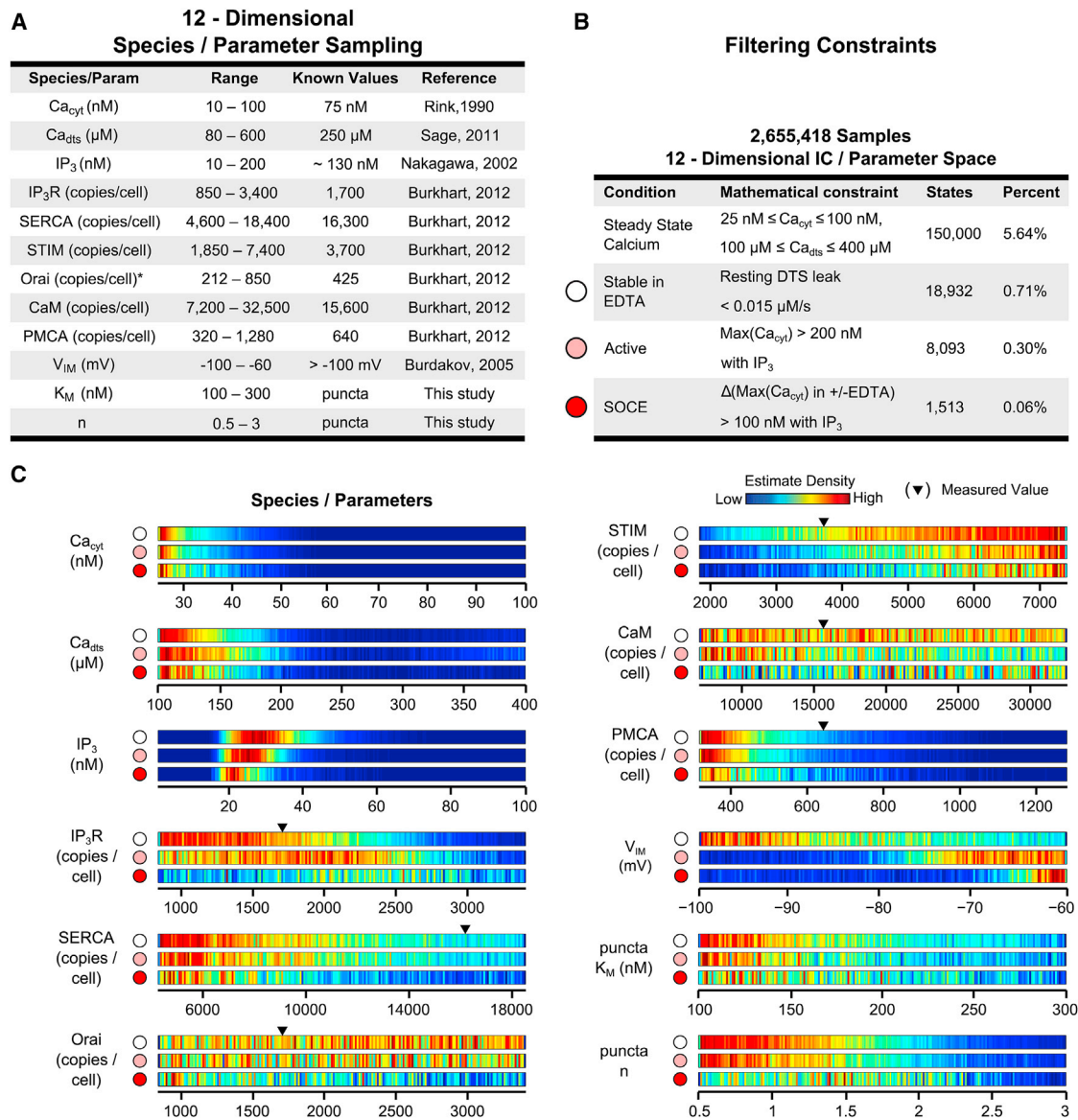


FIGURE 3 Dense initial condition space scanning reveals topologically enforced homeostatic constraints. (A) 12-dimensional species and parameter space sampling ranges. (B) Resting configurations were divided into groups based on 1) resting $[Ca^{2+}]_{cyt}$ and $[Ca^{2+}]_{dts}$ being within physiologic ranges; 2) Ca^{2+} levels being stable upon Ca_{ex} removal; 3) active configurations in which $[Ca^{2+}]_{cyt}$ rises above 200 nM after 5.5-fold IP_3 stimulus; and 4) difference in $[Ca^{2+}]_{cyt}$ after 5.5-fold IP_3 stimulus with and without Ca_{ex} is at least 100 nM. Constraints are applied sequentially, e.g., resting configurations satisfying the SOCE constraint also satisfy those listed in the rows above. Percentages are relative to the initial set of 2,600,000 configurations. (C) Probability distributions of model species and parameter configurations satisfying the stable-in-EDTA, active, and SOCE filtering constraints. All distributions also satisfy the steady-state calcium criterion. (Arrow, top of first bar) Experimentally measured protein copy numbers (7).

The following constraints must be met by a dynamic model of Ca^{2+} regulation:

1. Maintain low cytoplasmic Ca^{2+} at rest in the presence of finite IP_3 levels;
2. Maintain high store concentration at rest, even in the absence of extracellular Ca^{2+} ;
3. Present an increase in cytoplasmic Ca^{2+} after stimulation; and
4. Refill the store after transient cellular activation.

To meet these requirements in the resting cell, PMCA pumping out of the cell must equal SOCE flux into the cell. Also, at rest, IP_3R flux must equal SERCA pumping. Importantly, placement of EDTA (Ca^{2+} chelator) outside a cell must not cause a rapid depletion of store Ca^{2+} . For example, platelets sitting in EDTA for 1 h can still mobilize Ca^{2+} after agonist stimulation. For platelets, resting Ca^{2+}_{cyt} is ~25–100 nM (9,44) and Ca^{2+}_{dts} is ~250 μM (45). At resting $[Ca^{2+}]_{cyt}$, SERCA likely cannot pump against concentrations higher than

500 μM Ca^{2+} , which places an upper limit on store Ca^{2+} levels (46).

We investigated which ICs and uncertain fixed parameters allow the model to satisfy the above four homeostatic and dynamic constraints. We performed a dense Monte Carlo sampling (5) over a uniform 12-dimensional space of several protein species (IP₃R, SERCA, STIM, Orai, CaM, and PMCA), nonprotein species ($[\text{Ca}^{2+}]_{\text{cyt}}$, $[\text{Ca}^{2+}]_{\text{dts}}$, [IP₃]), V_{IM} , and two unknown fixed parameters (K_m , n) in the model (see Fig. 3 A). For proteins, the search space was in a local region constrained by available liquid chromatography-mass spectrometry data (7). In general, copy numbers were allowed to vary by a factor of 2 above and below the measured value. Fixed quantities include: all other 84 rate parameters; V_{PM} (−60 mV); and $[\text{Ca}^{2+}]_{\text{ex}}$ (1.2 mM). Resting states were accepted based on $[\text{Ca}^{2+}]_{\text{cyt}}$ and $[\text{Ca}^{2+}]_{\text{dts}}$ satisfying the physiologic constraints outlined above.

A dense sampling of >2,600,000 ICs from this 12-dimensional sampling space produced 150,000 steady states that satisfied the homeostatic requirements placed on resting Ca^{2+} . An important additional resting criterion is that states remain stable upon Ca_{ex} removal; this is particularly important in the context of our modeling because Ca_{ex} chelation is an important experimental technique for measuring the contribution of extracellular Ca^{2+} entry (e.g., SOCE) to the overall Ca^{2+} response. To apply this condition, we selected states that exhibited <5 μM decline in $[\text{Ca}^{2+}]_{\text{dts}}$ over 333 s after Ca_{ex} removal. This constraint is supported by experiments in which cells did not respond to Ca^{2+} readdition after having been stored in EDTA for >10 min (implying their stores were not significantly drained) (47).

The set of accepted resting states were further characterized and separated based on their responses to an IP₃ stimulus: states that are responsive to IP₃ (peak $[\text{Ca}^{2+}]_{\text{cyt}} > 200$ nM) and states that are both responsive to IP₃ and exhibit SOCE (difference in peak $[\text{Ca}^{2+}]_{\text{cyt}}$ in simulations with and without Ca_{ex} is >100 nM). We chose to use $[\text{Ca}^{2+}]_{\text{cyt}}$ as the metric because this quantity is commonly measured and numerous data in the literature point to a substantial difference in $[\text{Ca}^{2+}]_{\text{cyt}}$ under agonist stimulation with and without Ca_{ex} present. These filtering criteria, which were applied sequentially, and the number of resting states that satisfy each, are tabulated in Fig. 3 B. Notably, <0.06% of all sampled ICs satisfied all four homeostatic and dynamic criteria, indicating that the system is well constrained by these criteria.

Fig. 3 C presents the probability distributions of each search dimension for the three filtered populations (i.e., functional phenotypes) of IC configurations (Fig. 3 B), all of which maintain stable resting $[\text{Ca}^{2+}]_{\text{cyt}}$ and $[\text{Ca}^{2+}]_{\text{dts}}$ as a requirement of the homeostasis assumption. Where applicable, an arrowhead indicates measured resting values. The model topology and parameterization and filtering criteria placed sufficient constraint to push resting $[\text{Ca}^{2+}]_{\text{cyt}}$ and $[\text{Ca}^{2+}]_{\text{dts}}$ to the lower end of the search range. Platelets

that met all criteria had IP₃ levels that were constrained fairly narrowly between 20 and 40 nM (<200 copies per platelet), somewhat lower than the measured 130-nM value (43). The model accepts lower $[\text{Ca}^{2+}]_{\text{dts}}$ than the measured value of ~250 μM (45). This is likely due to the constraints our sampling ranges have placed on the ratio of SERCA to IP₃R.

As of this writing, no experimental measurements of V_{IM} exist due to technical difficulties in measuring potential across the ER membrane using patch-clamp. We allowed our scans to sample V_{IM} in the range of −100 to −60 mV based on the arguments presented in Methods. Model configurations stable in EDTA show a lower inner membrane potential; however, in stark contrast, configurations that are responsive to IP₃ and demonstrate SOCE possess a higher V_{IM} that clusters near the upper bound of the sampling range. The parameters n and K_M , which govern STIM₂ entry into puncta, become more monodisperse as additional filtering conditions are applied.

Calcium dynamics during agonist stimulation

Calcium release from the stores requires transient stimulation of IP₃R by IP₃. Literature measurements of IP₃ time courses in human platelets stimulated by strong doses of agonists such as thrombin and ADP show [IP₃] rising sharply by severalfold and peaking within 2.5–30 s after agonist delivery (41–43). Furthermore, [IP₃] and $[\text{Ca}^{2+}]_{\text{cyt}}$ return to nearly resting levels 30–60 s after agonist stimulation (48) as IP₃ is degraded by phosphatases and Ca^{2+} is pumped back into the DTS. Fig. 4 A shows the response of a subset of the fully filtered population of resting states to an IP₃ stimulus constructed to mimic these measured behaviors. $[\text{Ca}^{2+}]_{\text{cyt}}$ generally peaks within 15–20 s of IP₃ application. The [IP₃] time courses that are shown in the inset peak ~3 s after application; each state has a slightly different [IP₃] time course as their resting levels of IP₃ vary. $[\text{Ca}^{2+}]_{\text{cyt}}$ reaches a higher peak and remains more sustained in the presence of extracellular Ca^{2+} . $[\text{Ca}^{2+}]_{\text{dts}}$ partially refills in simulations run with Ca_{ex} and shows no refilling in calcium-free media. $[\text{Ca}^{2+}]_{\text{cyt}}$ peaks earlier in simulations without Ca_{ex} ; this is due to SOCE continuing to be partially active as stores refill rather than there being a time delay in I_{SOC} activation after store depletion (see Fig. S3).

Fig. 4 B shows the Ca^{2+} responses of a representative configuration from the stable population to a series of increasing [IP₃] stimulations shown in the inset for $\pm\text{Ca}_{\text{ex}}$ conditions. The 1.5 \times and 2 \times stimulations were too weak to elicit substantial SOCE; at higher IP₃ doses, stores become depleted enough that SOCE manifests itself via elevated $[\text{Ca}^{2+}]_{\text{cyt}}$ and substantial store refilling. The model predicts faster time to peak $[\text{Ca}^{2+}]_{\text{cyt}}$ at stronger IP₃ doses in $-\text{Ca}_{\text{ex}}$ simulations; in contrast, in $+\text{Ca}_{\text{ex}}$ simulations, peak $[\text{Ca}^{2+}]_{\text{cyt}}$ is higher and delayed until stores refill to

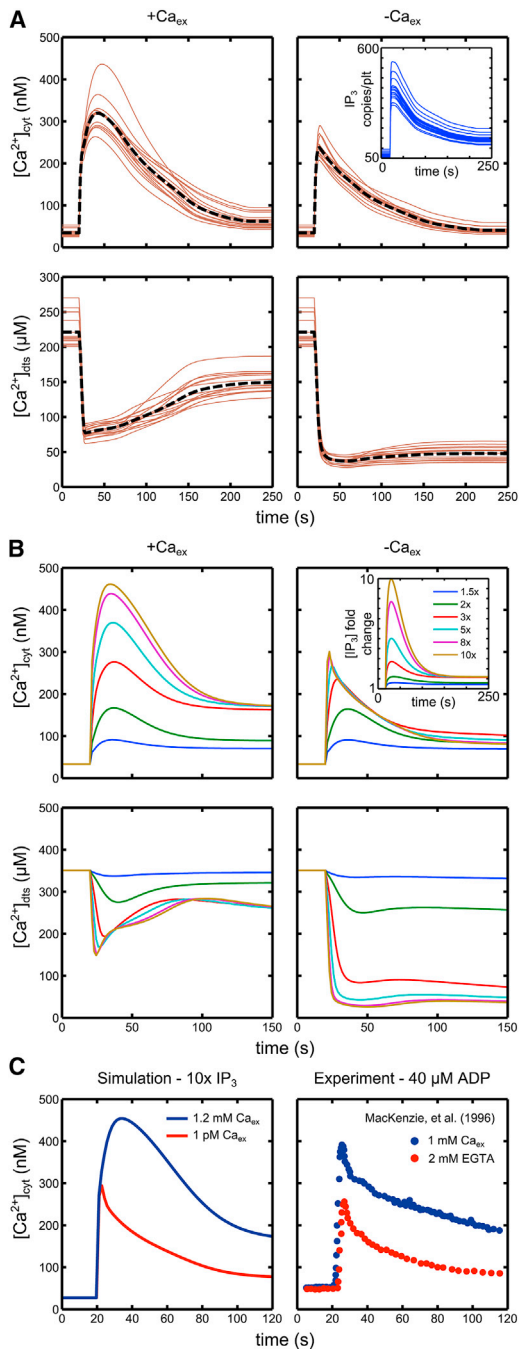


FIGURE 4 Model responses to IP₃ stimuli. (A) Fifteen resting configurations satisfying all filtering criteria were stimulated with 5.5-fold IP₃ dose starting at $t = 20$ s. (Inset, upper-right panel) IP₃ doses. (B) Calcium traces for DTS and cytosolic Ca²⁺ of a representative configuration taken from this population to the six IP₃ doses shown (inset, upper-right panel). The colors of the curves correspond to the IP₃ dose. (Left column) [Ca²⁺]_{ex} = 1.2 mM; (right column) [Ca²⁺]_{ex} = 1 pM. (C) Comparison of the 10× IP₃ simulations from panel B to calibrated fura-2 time-course data in human platelets treated with 40 μM ADP at $t = 20$ s (49).

sufficiently inactivate SOCE (also see Fig. S3). Fig. 4 C compares the model's response to the 10× IP₃ stimulation with time-course data from human PRP fluorescently

labeled with fura-2 and treated with 40 μM ADP (49). The simulated response is able to maintain good agreement with the data. In simulations run without Ca_{ex}, [Ca²⁺]_{cyt} peaks within 5 s and declines to baseline over a timescale of ~1 min (Fig. 4 C, red curve). In simulations run with Ca_{ex}, [Ca²⁺]_{cyt} peaks within 20 s after stimulus and remains elevated (Fig. 4 C, blue curve).

Fig. 5 A shows histograms of peak [Ca²⁺]_{cyt} after application of each dose of IP₃, shown in the inset of Fig. 4 B, to the entire set of stable configurations ($n = 18,932$). As the IP₃ dose is increased, more configurations in this population satisfy the active criterion (see Fig. 3 B). Stronger doses predictably result in higher average [Ca²⁺]_{cyt}; this effect saturates past 5× IP₃.

To assess the importance of puncta formation on the resting stability of the population of states satisfying all filtering criteria, the parameter α , which governs the maximum fraction of STIM₂ able to form puncta (see Eq. 2), was altered from the initial value of 0.2 to 0.5, 0.75, and 1. After allowing the states to relax to a new steady state, resting I_{SOC} was recorded; it is shown in Fig. 5 B. Increasing α increases the number of active (STIM₂)_p at rest and the constitutive I_{SOC} leak increases correspondingly; states with higher resting I_{SOC} lose Ca²⁺ more quickly after EDTA application. Therefore, as α is increased, fewer states satisfy the stability in EDTA criterion cutoff, which is indicated by the red dotted line drawn down all the histograms. The I_{SOC} cutoff is equivalent to the rate of change of [Ca²⁺]_{dts} criterion indicated in Fig. 3 B because PM Ca²⁺ flux is the rate-limiting step for Ca²⁺ leakage.

In Fig. 5 C, all model configurations in the stable in EDTA population were subjected to a 10× IP₃ dose at $t = 0$ s with [Ca²⁺]_{ex} set to 1.2 mM. Fig. 5 C (left) shows no correlation between the time at which [Ca²⁺]_{cyt} reaches its peak and the amount of fractional store refilling. Fig. 5 C (right) shows that the peak [Ca²⁺]_{cyt} time decreases as the SERCA to IP₃R ratio increases. Because SERCA and IP₃R act in direct opposition to one another, configurations with a higher SERCA/IP₃R are able to refill stores more quickly.

Clustering analysis

A hierarchical clustering analysis performed against a set of 13 model predictions recorded during IP₃ stimulation (see Fig. S4) reveals relationships between the model's dynamic emergent properties and the IC. Model predictions used in this analysis include peak [Ca²⁺]_{cyt}, time of peak [Ca²⁺]_{cyt}, minimum [Ca²⁺]_{dts}, total flux through each protein pump or channel, and the amount of store refilling after initial depletion. This clustering analysis was done on a random subset of the unfiltered resting configurations and divides this population into two main clusters, one enriched in configurations responsive to IP₃ and the other featuring dead platelets. The results reconfirm that high

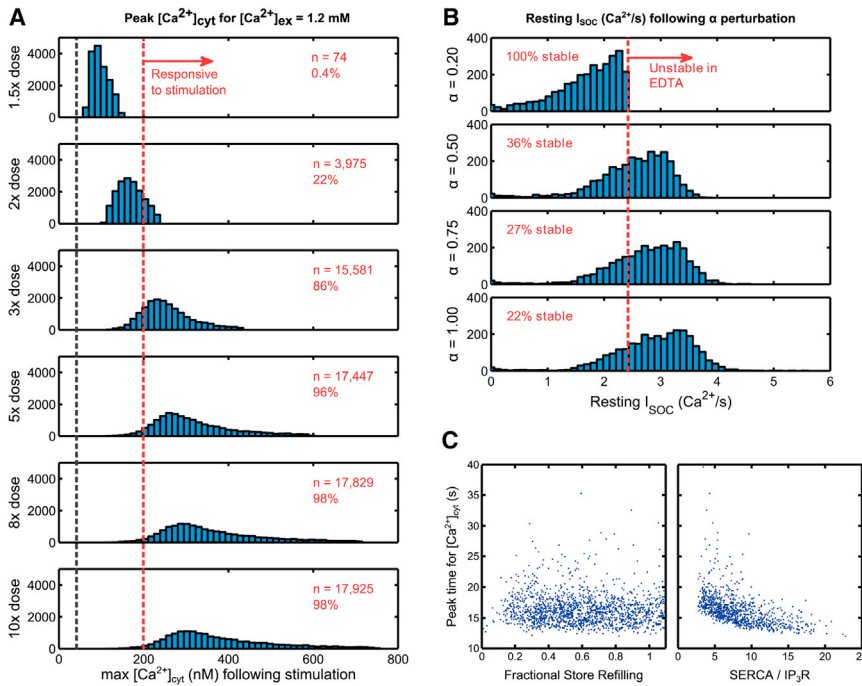


FIGURE 5 Model population behaviors. (A) The population of configurations satisfying the stability criterion ($n = 18,932$) were stimulated by the same doses of IP₃ as in Fig. 4 B and peak $[Ca^{2+}]_{cyt}$ for each state after the stimulus was recorded. The IP₃ stimulus begins at 10 s. (Black vertical dotted line) Mean resting $[Ca^{2+}]_{cyt}$; (red dotted line) cutoff for a configuration to be considered responsive to stimulus. (Upper-right of each histogram, in red) Number and percentage of configurations satisfying this criterion. (B) Population of configurations satisfying all filtering criteria ($n = 1513$) had the parameter α , which governs STIM1₂ puncta formation altered from 0.2 to 0.5, 0.75, and 1. Constitutive I_{SOC} leak increases as α is increased, leading to fewer states (red dotted line) that actually satisfy the stability criterion. (C) Model configurations in the stable population were subjected to a 10 \times IP₃ dose at $t = 0$ s with $[Ca^{2+}]_{ex}$ set to 1.2 mM. (Left panel) Scatter plot of the time at which $[Ca^{2+}]_{cyt}$ peaks, versus fractional amount of store refilling, reveals no correlation between the metrics. Fractional refilling is calculated as the final value of $[Ca^{2+}]_{dts}$ in a simulation divided by the initial drop after IP₃ stimulus. (Right panel) Scatter plot of the time at which $[Ca^{2+}]_{cyt}$ peaks versus SERCA/IP₃R.

V_{IM} is needed for a configuration to be responsive to IP₃. Configurations also exhibiting SOCE (cluster D in Fig. S4 A) are characterized by high amounts of IP₃R and CaM (see Fig. S4 B). A higher IP₃R/SERCA is important to allow Ca^{2+} to accumulate in the CYT instead of immediately getting pumped into the DTS. This group also possesses high levels of CaM, which indicates that CaM is important under activating conditions for modulating PMCA activity when SOCE flux is high. See the Supporting Material for additional details.

DISCUSSION

We have combined kinetic, mechanistic, and electrochemical data to produce a model of IP₃-mediated Ca^{2+} release and SOCE in human platelets that can estimate the resting and dynamic behavior of platelets in both calcium-containing and calcium-free conditions.

Multiple steady states (the 1513 ICs meeting the filtering criteria, Fig. 3, B and C) are expected and were sought out, because

1. Total protein measurements (Fig. 3 A) do not define the distribution of the antigen within the individual modules (Fig. 2) where the six measured protein levels for IP₃R, SERCA, STIM, Orai, CaM, and PMCA are actually distributed over 24 sub-species/complexes (see Table S1 in the Supporting Material) which are not known but must be consistent with the topology, kinetic parameters, homeostasis requirement, and filtering criteria;

2. Cellular heterogeneity is expected around a population average measurement and variations for a particular protein could easily be $\pm 100\%$ as explored in Fig. 3, A and C; and
3. The filtering criteria defined in Fig. 3 B are based upon ranges and upper and lower bounds, not strict values (e.g., steady state $[Ca^{2+}]_{cyt} = 75$ nM).

The IC exploration range was also fairly restricted for IP₃R, SERCA, Orai, STIM, CaM, and PMCA around their measured values (Fig. 3 C). The filtering criteria and model topology was more restrictive of allowed ICs for SERCA, STIM, and PMCA, but less so for IP₃R, Orai, and CaM, suggesting less model sensitivity to the values of IP₃R, Orai, and CaM; these broader distributions are also partly a consequence of the relatively narrow sampling ranges used in comparison to prior work (4). However, clustering analysis has revealed a role for high levels of CaM and IP₃R in the best-responder subset of the global steady-state population (see Fig. S4)—a fact not readily apparent from the distributions in Fig. 3 C.

Membrane electric potential is an important parameter for modeling channel current because it affects the driving force for passage of charged particles across a membrane. The potential across the inner membrane (V_{IM}) is largely unexplored because it is difficult to assess with traditional patch-clamp techniques (38). The value V_{IM} acts in opposition to the favorable Ca^{2+} concentration gradient across the IM, effectively acting as a brake on Ca^{2+} release and functionally placing a lower bound on $[Ca^{2+}]_{dts}$ by setting the Nernst potential at which Ca^{2+} flux out of the DTS via

IP_3R is zero (see Eq. 4). In agreement with this idea, in our model resting configurations satisfying only the static constraint of being stable in EDTA show a broad distribution of V_{IM} values. However, after application of the two dynamic constraints, V_{IM} clusters to the high (less-negative) end of the sampling range (see Fig. 3 C); a higher V_{IM} is evidently required to support the rate and amount of Ca^{2+} release required for platelet activation. In the future, incorporation of K^+ and Na^+ transport as well as cotransport of counterions with Ca^{2+} would allow for modeling of membrane potential transient behavior.

The requirement of a resting model configuration approximately remaining at steady state on Ca^{2+}_{ex} removal necessitates a low resting flux through SOCs. This is coupled with a requirement that, after activation, SOCE flux rises to levels that are sufficient to elevate $[Ca^{2+}]_{cyt}$ and effect store refilling. These points mean that a model for SOCE needs to have significant cooperativity with respect to decreases in $[Ca^{2+}]_{dts}$.

Cooperativity is introduced in three steps. The first is STIM oligomerization following loss of bound DTS Ca^{2+} which is well supported by experiments showing increases in STIM-STIM FRET following store depletion (6,50). The second facet of cooperativity comes from graded activation of Orai by association with multiple STIM dimers modeled with Eq. 3 (18). We model STIM- Ca_{dts} association and STIM dimerization with mass action kinetics; this leads to nonzero $STIM_2$ at rest even when stores are full. The third cooperative mechanism, enforcing $STIM_2$ needing to be in the puncta before being able to associate with Orai, is necessary for the model to both have a low enough resting I_{SOC} flux to be stable in EDTA and to simultaneously exhibit appreciable SOCE contribution to $[Ca^{2+}]_{cyt}$ following stimulus (see Fig. 5 B).

We see a small time delay in peak $[Ca^{2+}]_{cyt}$ of ~15 s compared to simulations run without Ca_{ex} (see Fig. 4). Fluorescently labeled human platelets stimulated with ADP show $[Ca^{2+}]_{cyt}$ peaking within 5–10 s of agonist addition and show little difference in peak time in calcium-containing versus calcium-free conditions (see right panel in Fig. 4 C) (49). However, some groups have observed in fluorescently labeled cells after application of thrombin, which is a stronger platelet agonist, a fast rise in $[Ca^{2+}]_{cyt}$ followed by a slower increase (51). In addition our own group routinely observes a time difference of ~20 s between agonist delivery and peak $[Ca^{2+}]_{cyt}$ in fluorescently labeled 10% PRP under calcium-free conditions (52).

Evidence for alternative regulation of SOCE inactivation has been observed in the literature. Studies have reported that CRACR2A, a transmembrane protein with a cytosol-facing EF-hand domain, may be responsible for stabilizing the STIM-Orai complex and that this effect is inhibited at high $[Ca^{2+}]_{cyt}$ (53). STIM also may be able to interact with phosphoinositides in the PM via its cytosolic polybasic domain. Inhibition of phosphatidylinositol 3- and 4-kinases

has been shown to reduce SOCE (54). However, PIP and PIP_2 levels do not change appreciably in thrombin-stimulated platelets (55). Additionally, many Ca^{2+} channels, including SOCs, are affected by the phenomena of Ca^{2+} -dependent inactivation (CDI) in which Ca^{2+} influx results in local domains of high $[Ca^{2+}]_{cyt}$, interfering with channel operation (6). This effect is independent of store refilling (56). In the future, modeling these regulatory mechanisms may allow for faster SOCE inactivation as stores refill.

Store refilling is often indirectly measured by observing changes in $[Ca^{2+}]_{cyt}$, $[Ca^{2+}]_{dts}$, or I_{SOC} after Ca^{2+} addition in cell populations where stores have been depleted with ionomycin and/or SERCA inhibitors such as thapsigargin (6,56,57); these studies are not reflective of store refilling during agonist stimulation. Only a few groups have directly measured $[Ca^{2+}]_{dts}$ versus time in human platelets, which is because most fluorescent Ca^{2+} sensitive dyes are higher affinity dyes designed to measure $[Ca^{2+}]_{cyt}$. One group has used Fluo-5N to measure $[Ca^{2+}]_{dts}$ in human platelets after stimulation with ADP and thrombin, among other compounds (45). In the absence of Ca^{2+}_{ex} , no store refilling was observed after addition of these agonists; our model is consistent with these measurements (see Fig. 4). This same group observed fast (within 30 s of agonist addition) but partial refilling when thrombin was added to platelets in calcified media. Under strong IP_3 stimulus with Ca^{2+}_{ex} , our model is capable of 0–>100% store refilling depending on the resting configuration.

In Fig. 5 C (left panel), we see the model does not show the amount of fractional refilling of stores being correlated with peak $[Ca^{2+}]_{cyt}$ time. However, Fig. 5 C (right panel) does show a correlation with SERCA/ IP_3R . Taken together with the time courses shown in Fig. S3, this implies that, to avoid a significant time delay in peak $[Ca^{2+}]_{cyt}$, the stores need to refill quickly only to a level such that PMCA can overtake the SOCE flux rather than needing to refill completely. CDI could be modeled to directly effect a faster store refilling in early times after activation because high $[Ca^{2+}]_{cyt}$ in puncta microdomains also results in faster SERCA activity in those regions; this scheme would create a scenario of fast store refilling and CDI-dependent inactivation followed by a slower inactivation phase (perhaps dependent on residual store refilling and CRACR2A destabilization) that may be important for fully shutting off I_{SOC} in model configurations where stores only partially refill.

CONCLUSION

Our model is the first to our knowledge to incorporate a complete mechanism for SOCE into a larger-scale model of Ca^{2+} signaling. The model predicts that values of V_{IM} , an experimentally inaccessible quantity, need to be >-70 mV to achieve calcium release after agonist stimulation. Given the complexity of calcium regulation in biological systems,

a cellular signaling model will likely never be fully complete. In the future, incorporating additional experimental data will allow for more tightly distributed protein copies and will enable the inclusion of downstream platelet functionality such as granule secretion, integrin activation, and phosphatidylserine exposure as well as the modeling of receptors for other important platelet agonists such as thrombin and thromboxane.

SUPPORTING MATERIAL

Four figures, one table, and supplemental information are available at [http://www.biophysj.org/biophysj/supplemental/S0006-3495\(14\)00328-2](http://www.biophysj.org/biophysj/supplemental/S0006-3495(14)00328-2).

This work was funded by the National Institutes of Health under grant No. R01-HL-56621 (to S.L.D.).

REFERENCES

1. Wu, M. M., R. M. Luik, and R. S. Lewis. 2007. Some assembly required: constructing the elementary units of store-operated Ca^{2+} entry. *Cell Calcium*. 42:163–172.
2. Varga-Szabo, D., A. Braun, ..., B. Nieswandt. 2008. The calcium sensor STIM1 is an essential mediator of arterial thrombosis and ischemic brain infarction. *J. Exp. Med.* 205:1583–1591.
3. Nakamura, L., K. Sandrock-Lang, ..., B. Zieger. 2013. Platelet secretion defect in a patient with stromal interaction molecule 1 deficiency. *Blood*. 122:3696–3698.
4. Purvis, J. E., M. S. Chatterjee, ..., S. L. Diamond. 2008. A molecular signaling model of platelet phosphoinositide and calcium regulation during homeostasis and P2Y1 activation. *Blood*. 112:4069–4079.
5. Purvis, J. E., R. Radhakrishnan, and S. L. Diamond. 2009. Steady-state kinetic modeling constrains cellular resting states and dynamic behavior. *PLoS Comput. Biol.* 5:e1000298.
6. Lewis, R. S. 2011. Store-operated calcium channels: new perspectives on mechanism and function. *Cold Spring Harb. Perspect. Biol.* <http://dx.doi.org/10.1101/cshperspect.a003970>.
7. Burkhart, J. M., M. Vaudel, ..., R. P. Zahedi. 2012. The first comprehensive and quantitative analysis of human platelet protein composition allows the comparative analysis of structural and functional pathways. *Blood*. 120:e73–e82.
8. Kholodenko, B. N., O. V. Demin, ..., J. B. Hoek. 1999. Quantification of short term signaling by the epidermal growth factor receptor. *J. Biol. Chem.* 274:30169–30181.
9. Heemskerck, J. W., G. M. Willems, ..., S. O. Sage. 2001. Ragged spiking of free calcium in ADP-stimulated human platelets: regulation of puff-like calcium signals in vitro and ex vivo. *J. Physiol.* 535:625–635.
10. Schmidt, H., and M. Jirstrand. 2006. Systems Biology Toolbox for MATLAB: a computational platform for research in systems biology. *Bioinformatics*. 22:514–515.
11. Dode, L., B. Vilsen, ..., J. P. Andersen. 2002. Dissection of the functional differences between sarco(endo)plasmic reticulum Ca^{2+} -ATPase (SERCA) 1 and 3 isoforms by steady-state and transient kinetic analyses. *J. Biol. Chem.* 277:45579–45591.
12. Sneyd, J., and J. F. Dufour. 2002. A dynamic model of the type-2 inositol trisphosphate receptor. *Proc. Natl. Acad. Sci. USA*. 99:2398–2403.
13. Dean, W. L., D. Chen, ..., T. C. Vanaman. 1997. Regulation of platelet plasma membrane Ca^{2+} -ATPase by cAMP-dependent and tyrosine phosphorylation. *J. Biol. Chem.* 272:15113–15119.
14. Caride, A. J., A. G. Filoteo, ..., E. E. Strehler. 2007. The plasma membrane Ca^{2+} pump isoform 4a differs from isoform 4b in the mechanism of calmodulin binding and activation kinetics: implications for Ca^{2+} signaling. *J. Biol. Chem.* 282:25640–25648.
15. Brini, M., and E. Carafoli. 2011. The plasma membrane Ca^{2+} ATPase and the plasma membrane sodium calcium exchanger cooperate in the regulation of cell calcium. *Cold Spring Harb. Perspect. Biol.* <http://dx.doi.org/10.1101/cshperspect.a004168>.
16. White, J. G. 2007. Platelet structure. In *Platelets* Elsevier, New York, pp. 45–73.
17. Ebbeling, L., C. Robertson, ..., J. M. Gerrard. 1992. Rapid ultrastructural changes in the dense tubular system following platelet activation. *Blood*. 80:718–723.
18. Hoover, P. J., and R. S. Lewis. 2011. Stoichiometric requirements for trapping and gating of Ca^{2+} release-activated Ca^{2+} (CRAC) channels by stromal interaction molecule 1 (STIM1). *Proc. Natl. Acad. Sci. USA*. 108:13299–13304.
19. Liou, J., M. L. Kim, ..., T. Meyer. 2005. STIM is a Ca^{2+} sensor essential for Ca^{2+} -store-depletion-triggered Ca^{2+} influx. *Curr. Biol.* 15:1235–1241.
20. Roos, J., P. J. DiGregorio, ..., K. A. Stauderman. 2005. STIM1, an essential and conserved component of store-operated Ca^{2+} channel function. *J. Cell Biol.* 169:435–445.
21. Luik, R. M., B. Wang, ..., R. S. Lewis. 2008. Oligomerization of STIM1 couples ER calcium depletion to CRAC channel activation. *Nature*. 454:538–542.
22. Varga-Szabo, D., A. Braun, and B. Nieswandt. 2011. STIM and Orai in platelet function. *Cell Calcium*. 50:270–278.
23. Muik, M., I. Frischauf, ..., C. Romanin. 2008. Dynamic coupling of the putative coiled-coil domain of Orai1 with STIM1 mediates Orai1 channel activation. *J. Biol. Chem.* 283:8014–8022.
24. Calloway, N., M. Vig, ..., B. Baird. 2009. Molecular clustering of STIM1 with Orai1/CRACM1 at the plasma membrane depends dynamically on depletion of Ca^{2+} stores and on electrostatic interactions. *Mol. Biol. Cell*. 20:389–399.
25. Liou, J., M. Fivaz, ..., T. Meyer. 2007. Live-cell imaging reveals sequential oligomerization and local plasma membrane targeting of stromal interaction molecule 1 after Ca^{2+} store depletion. *Proc. Natl. Acad. Sci. USA*. 104:9301–9306.
26. Barr, V. A., K. M. Bernot, ..., L. E. Samelson. 2009. Formation of STIM and Orai complexes: puncta and distal caps. *Immunol. Rev.* 231:148–159.
27. Rosado, J. A., S. Jenner, and S. O. Sage. 2000. A role for the actin cytoskeleton in the initiation and maintenance of store-mediated calcium entry in human platelets. Evidence for conformational coupling. *J. Biol. Chem.* 275:7527–7533.
28. Li, Z., L. Liu, ..., T. Xu. 2011. Graded activation of CRAC channel by binding of different numbers of STIM1 to Orai1 subunits. *Cell Res.* 21:305–315.
29. Monod, J., J. Wyman, and J. P. Changeux. 1965. On the nature of allosteric transitions: a plausible model. *J. Mol. Biol.* 12:88–118.
30. Alberts, B. 2002. *Molecular Biology of the Cell*. Garland Science, New York.
31. Hodgkin, A. L., and A. F. Huxley. 1990. A quantitative description of membrane current and its application to conduction and excitation in nerve. *Bull. Math. Biol.* 52:25–71.
32. Juska, A. 2010. Plasma membrane calcium pump and sodium-calcium exchanger in maintenance and control of calcium concentrations in platelets. *Biochem. Biophys. Res. Commun.* 392:41–46.
33. Adelman, W. J. 1971. *Biophysics and Physiology of Excitable Membranes*. Van Nostrand Reinhold, New York.
34. Mahaut-Smith, M. P., D. Thomas, ..., M. J. Mason. 2003. Properties of the demarcation membrane system in living rat megakaryocytes. *Biophys. J.* 84:2646–2654.
35. Mahaut-Smith, M. P., T. J. Rink, ..., S. O. Sage. 1990. Voltage-gated potassium channels and the control of membrane potential in human platelets. *J. Physiol.* 428:723–735.

36. Rink, T. J., and S. O. Sage. 1990. Calcium signaling in human platelets. *Annu. Rev. Physiol.* 52:431–449.
37. MacIntyre, D. E., and T. J. Rink. 1982. The role of platelet membrane potential in the initiation of platelet aggregation. *Thromb. Haemost.* 47:22–26.
38. Burdakov, D., O. H. Petersen, and A. Verkhratsky. 2005. Intraluminal calcium as a primary regulator of endoplasmic reticulum function. *Cell Calcium.* 38:303–310.
39. Mogami, H., A. V. Tepikin, and O. H. Petersen. 1998. Termination of cytosolic Ca^{2+} signals: Ca^{2+} reuptake into intracellular stores is regulated by the free Ca^{2+} concentration in the store lumen. *EMBO J.* 17:435–442.
40. Solovyova, N., N. Veselovsky, ..., A. Verkhratsky. 2002. Ca^{2+} dynamics in the lumen of the endoplasmic reticulum in sensory neurons: direct visualization of Ca^{2+} -induced Ca^{2+} release triggered by physiological Ca^{2+} entry. *EMBO J.* 21:622–630.
41. Tarver, A. P., W. G. King, and S. E. Rittenhouse. 1987. Inositol 1,4,5-trisphosphate and inositol 1,2-cyclic 4,5-trisphosphate are minor components of total mass of inositol trisphosphate in thrombin-stimulated platelets. Rapid formation of inositol 1,3,4-trisphosphate. *J. Biol. Chem.* 262:17268–17271.
42. Yang, X., L. Sun, ..., A. K. Rao. 1996. Human platelet signaling defect characterized by impaired production of inositol-1,4,5-trisphosphate and phosphatidic acid and diminished pleckstrin phosphorylation: evidence for defective phospholipase C activation. *Blood.* 88:1676–1683.
43. Nakagawa, T., H. Hirakata, ..., K. Fukuda. 2002. Ketamine suppresses platelet aggregation possibly by suppressed inositol triphosphate formation and subsequent suppression of cytosolic calcium increase. *Anesthesiology.* 96:1147–1152.
44. Siess, W. 1989. Molecular mechanisms of platelet activation. *Physiol. Rev.* 69:58–178.
45. Sage, S. O., N. Pugh, ..., A. G. Harper. 2011. Monitoring the intracellular store Ca^{2+} concentration in agonist-stimulated, intact human platelets by using Fluo-5N. *J. Thromb. Haemost.* 9:540–551.
46. Shannon, T. R., K. S. Ginsburg, and D. M. Bers. 2000. Reverse mode of the sarcoplasmic reticulum calcium pump and load-dependent cytosolic calcium decline in voltage-clamped cardiac ventricular myocytes. *Biophys. J.* 78:322–333.
47. Bird, G. S., W. I. DeHaven, ..., J. W. Putney, Jr. 2008. Methods for studying store-operated calcium entry. *Methods.* 46:204–212.
48. Daniel, J. L., C. Dangelmaier, ..., S. P. Kunapuli. 1998. Molecular basis for ADP-induced platelet activation. I. Evidence for three distinct ADP receptors on human platelets. *J. Biol. Chem.* 273:2024–2029.
49. MacKenzie, A. B., M. P. Mahaut-Smith, and S. O. Sage. 1996. Activation of receptor-operated cation channels via P2X1 not P2T purinoceptors in human platelets. *J. Biol. Chem.* 271:2879–2881.
50. Zhou, Y., P. Srinivasan, ..., P. G. Hogan. 2013. Initial activation of STIM1, the regulator of store-operated calcium entry. *Nat. Struct. Mol. Biol.* 20:973–981.
51. Harper, M. T., and A. W. Poole. 2011. Store-operated calcium entry and non-capacitative calcium entry have distinct roles in thrombin-induced calcium signaling in human platelets. *Cell Calcium.* 50:351–358.
52. Chatterjee, M. S., J. E. Purvis, ..., S. L. Diamond. 2010. Pairwise agonist scanning predicts cellular signaling responses to combinatorial stimuli. *Nat. Biotechnol.* 28:727–732.
53. Srikanth, S., H.-J. Jung, ..., Y. Gwack. 2010. A novel EF-hand protein, CRACR2A, is a cytosolic Ca^{2+} sensor that stabilizes CRAC channels in T cells. *Nat. Cell Biol.* 12:436–446.
54. Rosado, J. A., and S. O. Sage. 2000. Regulation of plasma membrane Ca^{2+} -ATPase by small GTPases and phosphoinositides in human platelets. *J. Biol. Chem.* 275:19529–19535.
55. Wilson, D. B., E. J. Neufeld, and P. W. Majerus. 1985. Phosphoinositide interconversion in thrombin-stimulated human platelets. *J. Biol. Chem.* 260:1046–1051.
56. Parekh, A. B., and J. W. Putney, Jr. 2005. Store-operated calcium channels. *Physiol. Rev.* 85:757–810.
57. Brini, M., D. Bano, ..., E. Carafoli. 2000. Effects of PMCA and SERCA pump overexpression on the kinetics of cell Ca^{2+} signaling. *EMBO J.* 19:4926–4935.